Development of a non-intrusive and efficient flow monitoring technique: the space-time image velocimetry (STIV)

ICHIRO FUJITA, Professor, Department of Architecture and Civil Engineering, Kobe University, 1-1 Rokkodai-cho, Nada-Ku, Kobe, 657-8501, Japan
Japan, Tel.: +81-78-803-6439, Fax: +81-78-803-6439, E-mail: ifujita@kobe-u.ac.jp, URL:http://www.kobe-u.ac.jp/c5labo

HIDEKI WATANABE, Graduate student, Graduate School of Science and Technology, Kobe University, 1-1 Rokkodai-cho, Nada-Ku, Kobe, 657-8501, Japan

RYOTA TSUBAKI, Doctoral student, Graduate School of Science and Technology, Kobe University, 1-1 Rokkodai-cho, Nada-Ku, Kobe, 657-8501, Japan

ABSTRACT
A novel image analysis technique for measuring river surface flow is proposed. When we assume that the brightness distribution of river surface image is convected with the surface velocity, a space-time image for a searching line set parallel to the main flow would indicate velocity information as its image orientation. The new technique, the space-time image velocimetry (STIV), is capable to measure the orientation angle of the pattern using the eigenvalue analysis of the local space-time image. The performance of STIV is compared with the other image analysis technique, the large-scale particle image velocimetry (LSPIV), previously proposed by the authors and it is shown that STIV is an alternative image analysis method for measuring streamwise velocity distributions efficiently.

Keywords: River flow measurement; Image analysis; Space-time image velocimetry (STIV); Large-scale image velocimetry (LSPIV); Real time measurement

1. Introduction

The measurement of river flow discharge in natural flow condition is one of the most difficult hydraulic measurements in river engineering especially during floods. Conventionally flood discharges have been gauged by measuring the time for several floats to pass through two measuring sections, however its accuracy is sometimes questionable when a float is trapped by a locally generated vortex

and tends to meander near the bank when passing through the measuring sections. The float length and the correction factor for converting float speed to the local depth-averaged flow velocity also involve some uncertainty because of the flow structure complexity during floods. Furthermore, the measurement work itself becomes dangerous in the case of a very large flood. Actually, there was an accident in September 2005 in Japan that a worker fell in a river while measuring flood discharge using floats. It is certain that sophisticated 2D or 3D flow measurement instrument such as Acoustic Doppler Current Profiler (ADCP) have become available for discharge measurements (Gordon, 1989), however ADCP cannot always be used from an economic viewpoint and it is also difficult to be used in an extreme flood.

In view of the previously mentioned status of flood flow measurements, Kinoshita (1967), Kinoshita et al. (1990), Utami et al. (1992), and Yamazaki et al. (1998) used aerial photographs to measure instantaneous spatial surface flow structure. Taguchi and Tsuru (1998) used images from a high resolution video camera, HDTV, in place of aerial photographs. Fujita and Komura (1994) developed a non-intrusive surface flow measurement method that utilizes video images taken from a riverbank or a bridge. The method is termed the large-scale particle image velocimetry (LSPIV) by Fujita, Muste and Kruger (1998), as this method is capable to cover a width of one hundred meters or more. Until now, LSPIV has been widely used for the measurements of river flows in the field and laboratory flumes: e.g. Fujita, Aya and Deguchi (1997), Fujita and Kawamura (2001), Aya et al. (2001), Bradley et al. (2002), Ettema et al. (1997), Creutin et al. (2003), Mezelhe et al.(2004) and Muste et al. (2004). A quasi-real time measurement system based on LSPIV is also available (Kruger et al. 2000). However, LSPIV has some shortcomings in its efficiency; for example, it requires a large storage memory for saving hundreds of large-sized images after the geometrical image correction in order to obtain mean flow quantities. LSPIV also requires a powerful CPU for the calculation of cross-correlation coefficients for the pattern matching in order to conduct the image analysis efficiently. Another disadvantage of LSPIV is that its spatial resolution becomes relatively low when the images are taken from a small depression angle. Therefore, the measurement accuracy becomes relatively lower farther from the viewing location due to the decrease of spatial resolution in the obliquely-viewed image. In addition, image-sampling frequency has to be chosen carefully in order to obtain reliable data in LSPIV. On the other hand, the proposed method is capable to resolve most of the above problems in a practical sense as will be discussed in the following sections.

2 Outline of space-time image velocimetry (STIV)

2.1 Generation of space-time image

The STIV utilizes a space-time image (STI) generated from time-change of brightness variation in a searching line set parallel to the main flow direction. The significant requirement of STIV is that there should appear a variation of brightness or color on the water surface moving with the surface flow. As an example of STI generation, the line segment indicated in the middle of Figure 1(a) is used in the following. The image is shot from a forty-meter-height deck of an observation tower located near the river. The spacing between the groins indicated in the figure is about 40 meters and the width of the river is about 60 meters. It is apparent from Figure 1(a), that the water surface exhibits a large-scale brightness variation. This variation is mainly caused by surface ripples generated by the confliction of boil vortices against the water surface. From a visual observation at the site, generation of boil vortices and the accompanied convection of the surface pattern can be easily detected. It was confirmed that the convection speed of the surface pattern agrees well with the surface floating tracers. The space-time expression of the brightness evolution in the line segment (searching line) indicated in Figure 1(a) is provided in Figure 1(b) as an STI. The STI, in this case, is formed by picking up the brightness information of the line segment from 180 consecutive image frames, which correspond to six seconds in time. The length of the line segment is 200 pixels with an actual length of 18.87m on the water surface. Obviously, the STI includes a pattern inclined towards the lower right corner. If we draw a line parallel to the pattern manually as indicated in Figure 1(b), the angle ϕ becomes about 68 degrees. From the above information, we can simply calculate that the convective velocity of the brightness distribution in the line segment, which is about 1.07m/s. The numerical value of this velocity is reasonable for the surface flow that should appear at this location. It should be noted that the obtained velocity is not an instantaneous velocity but the time-averaged velocity on the line segment even for a short time indicated in the above example. The actual mean velocity in the field condition can be obtained by using more consecutive images, i.e., by taking a longer averaging time to ensure the statistical numerical stability.

Another example is a flume flow visualized by surface tracers. Figure 2 shows a visualized surface flow viewed from an oblique angle and the STI for the line segment indicated in the figure. In this case, the line segment is intentionally provided so that it includes part of the block, assuming the case in which some part of the view is obstructed. Figure 2(b) obviously displays part of the block as a uniform gray zone together with a clear striped pattern indicating the flow. Manual inspection of the oblique angle gives an angle of minus 19 degrees, which yields a velocity of 0.44m/s. This value is a reasonable estimation and agrees with the hydraulic conditions of the flume.

The final example is the flood flow of the Uono River which occurred during the snowmelt in April.

Figure 3 shows the surface image together with ten searching lines. The water surface is subject to irregular deformation due to the effects of intense turbulence generated by the interaction between the riverbed and the water surface. The length of the line segment indicated in Figure 3 is 200 pixels and the STIs for each line segment are shown in Figure 4. Although the pattern is less clear than the previous cases, there appears a pattern having an orientation which indicates the water surface convection. It should be noted that the horizontal length of the respective STI is not constant because of the image obliqueness.

As mentioned above, once a STI displays a pattern with some orientation we can extract velocity information by measuring the mean orientation angle of the pattern. Therefore, if we were able to measure such an angle with a reasonable accuracy from each STI, without manual operation, it would become a practical and efficient method for measuring velocity distributions of river surface flows.

2.2 Orientation analysis of local neighborhood of STI

In the development of texture image analysis in the past decade, Jahne (1993) introduced a method for measuring a local image pattern. In the analysis, a parameter to measure the orientation angle is chosen as

$$F(\underline{x}) = \left(\nabla g(\underline{x})^T \underline{n}\right)^2 = |\nabla g|^2 \cos^2\left(\angle(\nabla g, \underline{n})\right) \tag{1}$$

where $g(\underline{x})$ denotes the gray level intensity (brightness) variation, $\underline{n}$ is a unit vector perpendicular to the lines of constant gray values or the orientation vector, ∇g represents the image gradient vector, the symbol $\angle$ denotes the angle between the vectors in the parentheses, and $\underline{x} = (x, t)$ is the coordinate system of STI. Here, the underlined variables indicate they are vector values. Since this quantity $F(\underline{x})$ is proportional to the cosine squared of the angle between the gradient vector and the orientation vector, it takes the maximum value when the two vectors are parallel or antiparallel and it becomes zero if they are perpendicular to each other. Therefore, when we pay attention to a local area (or a local neighborhood) in the image, the following integral should be maximized to obtain the appropriate orientation vector:

$$\int w(\underline{x} - \underline{x}') F(\underline{x}') d\underline{x}' = \underline{n}^T J \underline{n} \tag{2}$$

with

$$J = \int w(\underline{x} - \underline{x}') \left(\nabla g(\underline{x}') \nabla g(\underline{x}')^T\right) d\underline{x}', \tag{3}$$

where $\underline{x}'$ denotes the local coordinate system and the window function w determines the size and shape of the neighborhood around a point $\underline{x}$ in which the orientation is averaged. The component of J is

$$J_{pq}(\underline{x}) = \int w(\underline{x} - \underline{x}') \left(\frac{\partial g(\underline{x}')}{\partial x_p'} \frac{\partial g(\underline{x}')}{\partial x_q'} \right) d\underline{x}' \tag{4}$$

which is designated as the structure tensor. The suffixes p and q are indices representing either x or t. The maximization of eq.(2) can be performed by rotating the structure tensor into the principal axes coordinate systems:

$$\begin{aligned} \begin{bmatrix} \lambda_1 & 0 \\ 0 & \lambda_2 \end{bmatrix} &= \begin{bmatrix} \cos\phi & -\sin\phi \\ \sin\phi & \cos\phi \end{bmatrix} \begin{bmatrix} J_{xx} & J_{xt} \\ J_{xt} & J_{tt} \end{bmatrix} \begin{bmatrix} \cos\phi & \sin\phi \\ -\sin\phi & \cos\phi \end{bmatrix} \\ &= \begin{bmatrix} J_{xx}\cos^2\phi + J_{tt}\sin^2\phi - J_{xt}\sin 2\phi & \frac{1}{2}(J_{xx} - J_{tt})\sin 2\phi + J_{xt}\cos 2\phi \\ \frac{1}{2}(J_{xx} - J_{tt})\sin 2\phi + J_{xt}\cos 2\phi & J_{xx}\sin^2\phi + J_{tt}\cos^2\phi + J_{xt}\sin 2\phi \end{bmatrix} \end{aligned} \tag{5}$$

where λ_1 and λ_2 are the eigenvalues of the structure tensor. The orientation angle can be obtained by comparing the off-diagonal elements as

$$\tan 2\phi = \frac{2J_{xt}}{J_{tt} - J_{xx}} \tag{6}$$

where, with A indicating the local area in which the window function is applied,

$$J_{xx} = \int_A \frac{\partial g}{\partial x}\frac{\partial g}{\partial x} dxdx, \quad J_{xt} = \int_A \frac{\partial g}{\partial x}\frac{\partial g}{\partial t} dxdt, \quad \text{and} \quad J_{tt} = \int_A \frac{\partial g}{\partial t}\frac{\partial g}{\partial t} dtdt. \tag{7,8,9}$$

Thus the orientation vector $\underline{o}$ becomes

$$\underline{o} = \begin{bmatrix} J_{tt} - J_{xx} \\ 2J_{xt} \end{bmatrix}. \tag{10}$$

The advantageous aspect of the present method is that we can introduce a parameter termed the coherency C, which is a measure of coherence of image pattern and defined by

$$C = \frac{\sqrt{(J_{tt} - J_{xx})^2 + 4J^2{}_{xt}}}{J_{xx} + J_{tt}} = \frac{\lambda_1 - \lambda_2}{\lambda_1 + \lambda_2}. \tag{11}$$

The value of coherency changes from 0 to 1. For ideal local orientation ($\lambda_1 > 0$, $\lambda_2 = 0$) it becomes one and for an isotropic gray value structure ($\lambda_1 = \lambda_2 > 0$) it becomes zero. Therefore it is possible to pickup only the clear orientation information by referring to the coherence value.

In the present study, we calculate the image gradient using the forth order or the fifth order central difference schemes. For example, the image gradient in the space direction can be calculated by the forth order scheme

$$\frac{\partial g}{\partial x} = \frac{g_{i+2} - 8g_{i+1} + 8g_{i-1} - g_{i-2}}{12\Delta x} \tag{12}$$

or by the fifth order scheme

$$\frac{\partial g}{\partial x} = \frac{g_{i+3} - 9g_{i+2} + 45(g_{i+1} - g_{i-1}) - 9g_{i-2} - g_{i-3}}{60\Delta x}, \tag{13}$$

in which Δx is unity for a pixel image field.

Figure 5 illustrates briefly the procedure of STIV. Firstly, generate the space-time image (STI) for a searching line segment from N original images with a time spacing of Δt. Secondly, set a local window in the STI and calculate the image gradients of gray level intensity $g(x', t')$ with respect to space and time within the local window by using eq.(12) or eq.13. Thirdly, calculate the orientation angle within the local window from eqs.(6)-(9). Finally, calculate the mean orientation angle from the orientation angles obtained for the local windows being placed to cover the entire STI. The value of coherency obtained for each local window is used as a weight to calculate the mean value as will be explained in the following section. The idea of using coherency is to pick up reliable orientation angles with a clear pattern within the local window.

2.3 Evaluation of STIV using synthetic images

In order to examine the accuracy of the method, synthetic images with striped pattern having a specified orientation are analyzed and compared. For representing different water surface conditions, images with vague pattern (Case V) and those with clear pattern (Case C) are prepared by changing the orientation angle, $\tan\phi$, from 0.1(5.7degrees) to seven (81.9degrees). The image for the case $\tan\phi = 3$ is shown in Figure 6. The image size is 200 by 50 pixels. The images are generated by randomly superposing the Gaussian distribution with random mean and variance values.

The results of the orientation angle calculated by STIV are compared with the specified value as shown in Figure 7. The value of the coherency is more than 0.9 in these cases. It is obvious that the STIV yields highly accurate results for a wide range of orientation angle between $\tan\phi$ =0.1 (5.7degrees) and $\tan\phi$=7.0 (81.9degrees) in the Case V, while in the Case C the analyzed results become smaller than the specified value for the larger orientation angles. This error is due to the lack of smooth brightness distribution for the Case C. However, as indicated in Figure 7, the accuracy for the Case C is significantly improved by applying a smoothing filter, e.g. the Gaussian smoothing filter, to STI. This feature of STIV is crucial for developing a practical system because STIV does not necessarily require a high-resolution video camera for obtaining a reasonable result. The result

obtained herein implies that STIV has a large dynamic range in velocity measurements capable to detect a wide range of velocity distribution without changing any parameters. This aspect is completely different from LSPIV, in which measurement accuracy highly depends on image time spacing.

2.4 Method for calculating average orientation angle

In the actual application of STIV to river surface flows, the generated STI does not always contain a uniformly oriented pattern presented in the previous section; rather STI usually includes random background noise imbedded in a clear orientation pattern as indicated, for example, in Figure 4. For extracting meaningful information from such ambiguous space-time image, we can make use of the information of the coherency and the histogram of orientation distribution.

As an example, Figure 8 shows the analyzed results for the STI presented in Figure 1(b). The background image is enhanced for the sake of clarity. The white rectangle in the upper left corner, 31 by 31 pixels, is the local integration area A for calculating Eqs. (7)-(9). In the calculation of an orientation angle, the location of the integration area is shifted step by step while overlapping fifty percent of the respective area in this case. As can be seen clearly from Figure 8, there are several anomalous vectors in the middle zone of the STI, where the image quality for calculating an appropriate orientation vector is degraded. Figure 9 is the coherency distribution for the same STI as of Figure 8 or Figure 1(b). It is apparent that suitable orientation vectors are calculated only for the larger coherency area, while anomalous vectors appear in the area of low coherency.

In order to obtain a mean orientation angle, frequency distributions for several coherency ranges are utilized as shown in Figure 10. That is, the mean orientation angle $\bar{\phi}$ is calculated from the following equation

$$\bar{\phi} = \sum_{C=0}^{1.0} \frac{\sum_{\phi=\phi_{min}}^{\phi_{max}} \sum_{C_t=C}^{1.0} \phi \cdot W(\phi)}{\sum_{\phi=\phi_{min}}^{\phi_{max}} \sum_{C_t=C}^{1.0} W(\phi)} \quad , \tag{14}$$

where ϕ_{min} and ϕ_{max} indicate respectively the minimum and the maximum orientation angles arbitrarily chosen depending on the searching range of velocity, and $W(\phi)$ is the frequency distribution of the orientation angle used here as a weighting function. Figure 11 indicates the final frequency distribution used for calculating the weighted mean orientation angle. The idea behind eq. (14) is to count the orientation angle with larger coherency more frequently than the one with smaller coherency. It is seen clearly that the frequency distribution shown in Figure 11 has more sharply peaked shape than any of

the distribution in Figure 10. The parameters ϕ_{min} and ϕ_{max} can be used to discard the apparently erroneous vectors, which are caused by the hindering object shown in Figure 12.

2.5 Calculation of velocity component along line segment

Once the orientation angle is determined, the velocity component along the line segment can be calculated with the information on the physical length of the line segment calculated by the mapping relationship between the physical coordinates (X, Y, Z) and the screen coordinates (x, y). We used the following relation between the two coordinate systems:

$$\begin{aligned} x &= -c\frac{a_{11}(X-X_0)+a_{12}(Y-Y_0)+a_{13}(Z-Z_0)}{a_{31}(X-X_0)+a_{32}(Y-Y_0)+a_{33}(Z-Z_0)}+\Delta x \\ y &= -c\frac{a_{21}(X-X_0)+a_{22}(Y-Y_0)+a_{23}(Z-Z_0)}{a_{31}(X-X_0)+a_{32}(Y-Y_0)+a_{33}(Z-Z_0)}+\Delta y \end{aligned} \tag{15}$$

where (X_0, Y_0, Z_0) is the location of the camera, c is the focal length, a_{ij} (i,j=1,3) are the parameters indicating the direction of the camera and (Δx, Δy) denote the effect of lens distortion. The mapping relation can be established using the predetermined marker coordinates on both coordinate systems. With the above information together with the water level data, physical length of a line segment at the water surface can be easily calculated. Finally, the mean velocity component at the line segment can be simply provided by

$$U = \frac{S_x}{S_t}\tan\phi \tag{16}$$

where S_x (m/pixel) is the unit length scale of the line segment and S_t (sec/pixel) is the unit time scale of the time axis. S_t usually takes the value of 1/30 (sec/pixel) if we use the NTSC video system.

3 Outline of large-scale particle image velocimetry (LSPIV)

Before showing the application examples of STIV, the outline of the LSPIV is briefly presented here for comparison. In LSPIV, the mapping relation, eq.(15), also has to be established beforehand. The next step in LSPIV is to generate non-distorted images using eq.(15) with the water level information. Holland et al. (1997) used similar equations for image transformation to investigate wave-breaking

pattern in the nearshore zone. The size of the generated image depends on the size of the pixel, which can be arbitrarily chosen depending on the physical size of the target area. The point to note is to choose the pixel size so that the transformed image should have an image size comparable to or a little larger than the original image size. An example of the image transformation is shown in Figure 13. In this example, the original image is transformed taking a pixel size of 0.1m and the generated image has a size of 700 by 700 pixels. Once the transformed images are prepared, a conventional PIV (Raffel et al., 1997) can be applied to the images to measure two dimensional surface velocity distributions. A small rectangle indicated in Figure 13(b) shows the template size, 30 by 30 pixels, used for the template pattern matching in PIV.

4 Application of STIV and comparison with LSPIV

Several application examples of STIV are provided in the following together with the results from LSPIV. As has been pointed out, the most different feature of the two methods is that STIV measures the mean velocity component in the downstream direction while LSPIV measures two-dimensional instantaneous velocity components. Hence, depending on the objective of the measurements we may have to select either of the methods.

4.1 Laboratory flume flow measurement

A laboratory flume flow visualized by surface tracers with a mean diameter of 20 micrometers is videotaped from three angles. The image shown previously in Figure 2 corresponds to the angle B. Figure 14 indicates the images taken from the other two angles; the angle A is from above the flume and has no image distortion while the angle C is a view from the upstream location and has a relatively large image distortion. The blocks placed along the channel are used as mark points for establishing the mapping relationship. Measurement results for the same cross-section, which is indicated with the dashed line in Figure 2 and Figure 14 are presented in Figure 15. We used thirty seconds of images in each analysis; 900 consecutive frame images for STIV and 300 frame images with a time spacing of 0.1 seconds for PIV. The measurement results by STIV from three angles are compared with the result obtained by PIV from the angle A. It is clearly seen that velocity distributions obtained by STIV from three angles are in favorable agreement with LSPIV, although the angle C yields a little larger value than LSPIV in some part of the distribution, which may be due to a slight error in establishing the mapping relation.

4.2 Normal flow measurement The Uji River

Figure 16 shows the mainstream velocity distribution of the Uji River obtained at the section *y*=-22720m indicated in Figure 13. In the STIV analysis, thirty seconds of consecutive images are used. On the other hand, 150 images with a time spacing of 0.2 seconds are used in LSPIV. The reason for selecting time spacing different from the previous example is to improve the velocity resolution by increasing the relative pixel movement between two images. It is evident from Figure 15 that there is an excellent agreement between the two methods. Figure 17 shows the STIV result for the entire flow region that can be viewed from the observation tower. Here, the results from three angles are superposed to cover the rectangular region of 135 by 65 meters. Although the detailed flow structure such as flow reflection by the groins or shedding of vortices as reported by Fujita et al. (2004) cannot be captured by the present STIV analysis because STIV is a 1D measurement method, the general flow feature in the streamwise direction of the main flow, such as the acceleration of surface velocity due to the narrowing of the river channel width or the deceleration of velocity near the groins, is measured satisfactorily.

4.3 Flood flow measurement of the Uono River

The final example is for the flood flow of the Uono River already introduced in Figure 3. The analyzed results by STIV and LSPIV are compared in Figure 18. It can be seen clearly that the flood flow velocity is as high as 3.5m/s by using either of the methods and both method obtain almost the equivalent distribution. The point to note is since the riverbed becomes deeper nearer to the left bank according to a field survey, the measured result agrees well with the general feature of the velocity distribution at the measuring site. It should also be noted that surface flow measurement that covers a river width of one hundred meters can be performed by using only a single video camera placed at the river bank.

5 Conclusions

The new image analysis method proposed by the authors, STIV, is shown to be an efficient technique for river surface flow measurement, especially for the measurement of streamwise velocity distributions. The accuracy of the method is comparable to that of LSPIV previously proposed by the authors. The advantage of the method is that it can cover a measurement area of approximately one hundred meters, e.g. 135m by 65m in the case of the Uji River and a river width of 100m in the Uono River. It can also be noted that the spatial information presented in this paper is difficult to obtain by

other point measurement techniques. The other feature of STIV is its efficiency in the image analysis speed. According to a sample calculation performed by the authors, STIV is almost ten times faster than LSPIV to obtain the same amount of information, except that LSPIV is a two dimensional measurement method whereas STIV is a one dimensional measurement method in the streamwise direction. Therefore, STIV is not suitable for measuring recirculating flows which varies its direction with time but suitable for the velocity measurement of unidirectional flows where discharge measurements are usually performed. Table 1 summarizes the respective features of the two methods. In general, STIV should be mainly used for the observation of relatively straight flows or rather in a real-time manner in order to measure the river discharge, while LSPIV can be used to investigate more detailed flow features varying with time and space (Fujita, et al. 2004). As mentioned previously, in order for STIV or LSPIV to be successful in river flow measurements, there should appear some traceable image pattern or surface texture moving with the surface flow. Although the necessary hydraulic condition for their appearance is not clearly understood at present, at least when the river surface is influenced by the bottom turbulence we could detect such image pattern. However, it becomes difficult to apply the methods under the severe atmospheric conditions such as with appreciable wind waves or with heavy rain which blurs the images. Finally, it is worth noting that a quasi real-time flow monitoring system can be easily constructed with STIV or LSPIV where a river monitoring system such as a CCTV camera or a WEB camera is available near a river. The hydraulic information obtained by such monitoring system, together with the hydrologic data, would be of great help in constructing or refining hydrologic models for the efficient management of river basin.

Acknowlegements

The authors are grateful to the corporation by Dr. Muto in Kyoto University, Dr. Takehara and Dr. Takano in Kinki University, and Dr. Kanda in Akashi National College of Technology during the field measurements.

References

[1] Aya, S., Kakinoki, S., Aburaya, T. and Fujita, I. (2001). “Velocity and Turbulence Measurement of River Flows by LSPIV”, *Advances in Fluid Modelling & Turbulence Measurements* (*Proceeding of the 8th International Symposium on Flow Modeling and Turbulence Measurements*) (*FMTM2001*), 177-184.

[2] Bradley, A.A., Kruger, A., Meselhe, E, and Muste, M.(2002). ”Flow Measurement in Streams

Using Video Imagery", *Water Resources Research,* 38(12), 1315, doi:10.1029/2002WR001317.

[3] Creutin, J.D., Muste, M., Bradley, A.A., Kim, S.C. and Kruger, A. (2003), "River Gauging Using PIV Techniques: a Proof of Concept Experiment on Iowa River", *Journal of Hydrology,* 277, 182-194.

[4] Ettema, R., Fujita, I., Muste, M. and Kruger, A. (1997). "Particle-image Velocimetry for Whole-field Measurement of Ice Velocities", *Cold Regions Science and Technology,* 26, 97-112.

[5] Fujita, I., and Komura, S. (1994). "Application of Video Image Analysis for Measurements of River-Surface Flows", *Annual Journal of Hydraulic Engineering,* Japan Society of Civil Engineers, 38, 733-738, (in Japanese).

[6] Fujita, I., Aya, S. and Deguchi, T. (1997). "Surface Velocity Measurement of River Flow Using Video Images of an Oblique Angle", *Proceedings of the 27th Congress of IAHR,* Theme B, Vol.1, 227-232.

[7] Fujita, I., Muste, M. and Kruger, A. (1998). "Large-Scale Particle Image Velocimetry for Flow Analysis in Hydraulic Applications", *J. Hydr. Res*., 36(3), 397-414.

[8] Fujita, I. and Kawamura, Y. (2001). "Discharge Measurements of Flood Flow by Imaging Technology and Float Method", *Proceedings of the 29th Congress of IAHR,Theme D, Vol.*1,1-6.

[9] Fujita, I. and Tsubaki, R. (2002). "A Novel Free-Surface Velocity Measurement Method Using Spatiotemporal Images", *Hydraulic Measurements and Experimental Methods, ASCE,* on CDROM.

[10] Fujita,I., Muto, Y., Shimazu, Y., Tsubaki, R. and Aya, S. (2004). "Velocity Measurements Around Non-Submerged and Submerged Spur Dykes by means of Large-Scale Particle Image Velocimetry", *Journal of Hydroscience and Hydraulic Engineering, JSCE*, 22, No.1, 51-61.

[11] Gordon, L. (1989). "Acoustic Measurement of River Discharge", *J. Hydraulic Engineering,* 115, 925-936.

[12] Holland, T., Holman, R. A., and Lippmann, T. C. (1997). "Practical Use of Video Imagery in Nearshore Oceanographic Field Studies", *IEEE J. Oceanic Engineering,* 22(1), 81-95.

[13] Jahne, B. (1993). *Spatio-Temporal Image Processing*, Springer-Verlag, 150 -152.

[14] Kinoshita, R. (1967). "An Analysis of the Movement of Flood Waters by Aerial Photography Concerning Characteristics of Turbulence and Surface Flow", *Journal of the Japan Society of Photogrammetry*, 6(1), 1-17.

[15] Kinoshita, R., Utami, T. and Ueno, T. (1990). "Image Processing for Aerial Photographs of Flood Flow", *Photogrammetric Engineering & Remote Sensing,* 29(6), 4-17.

[16] Kruger, A., Bradley, A., Muste, M. and Fujita, I.(2000). "Real-Time Measurements of Free-Surface Velocity Using Imaging Techniques", *Hydroinformatics* 2000, on CDROM.

[17] Muste, M., Z. Xiong, J., Schöne, Z. Li. (2004). "Flow Diagnostic in Hydraulic Modeling Using

Image Velocimetry", *J. Hydraulic Engineering*, 130(3), 175-185.

[18] Meselhe, E. A., Peeva, T., and Muste, M. (2004). "Large Scale Particle Image Velocimetry for Low Flow and Shallow Water Flows", *J. Hydraulic. Engineering.*, 130(9), 937-940.

[19] Raffel, M., Willert, C., and Kompenhaus, J. (1997). Particle Image Velocimetry, Springer-Verlag.

[20] Taguchi, T. and Tsuru, K.(1998)."Analysis of Flood Flow by Stereomatching Method", *International Archives of Photogrammetry and Remote Sensing*, XXXII, 5, 810-813.

[21] Utami, T., Ueno, T. and Kinoshita, R. (1992). "A Study on the Turbulence Structure of Flood Flows and River Bed Forms Using the Picture Processing of Aerial Photographs", *Annuals of the Disaster Prevention Research Institute Kyoto University*, 35, B-2, 373-388.

[22] Yamazaki, F., Hatamoto, M. and Kondo, M. (1998)."Utilization of Synchronous Shutter Apparatus in the Photographic Measurement Method of Flood Flow Surface", *International Archives of Photogrammetry and Remote Sensing*, XXXII, 5, 848-855.

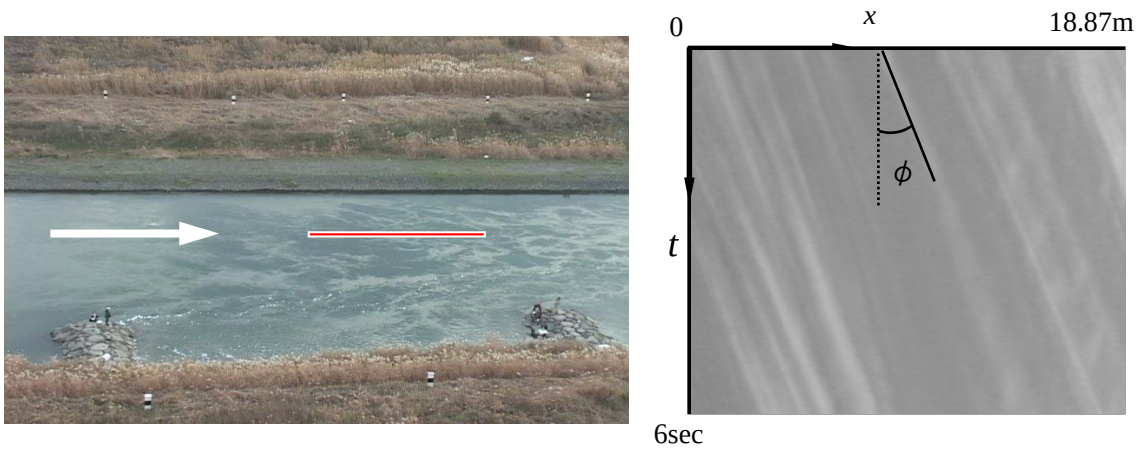

(a) (b)

Figure 1 River surface flow image of the Uji River; (a) oblique-angled image and a searching line (b) space-time expression of brightness distribution on the searching line indicated in (a).

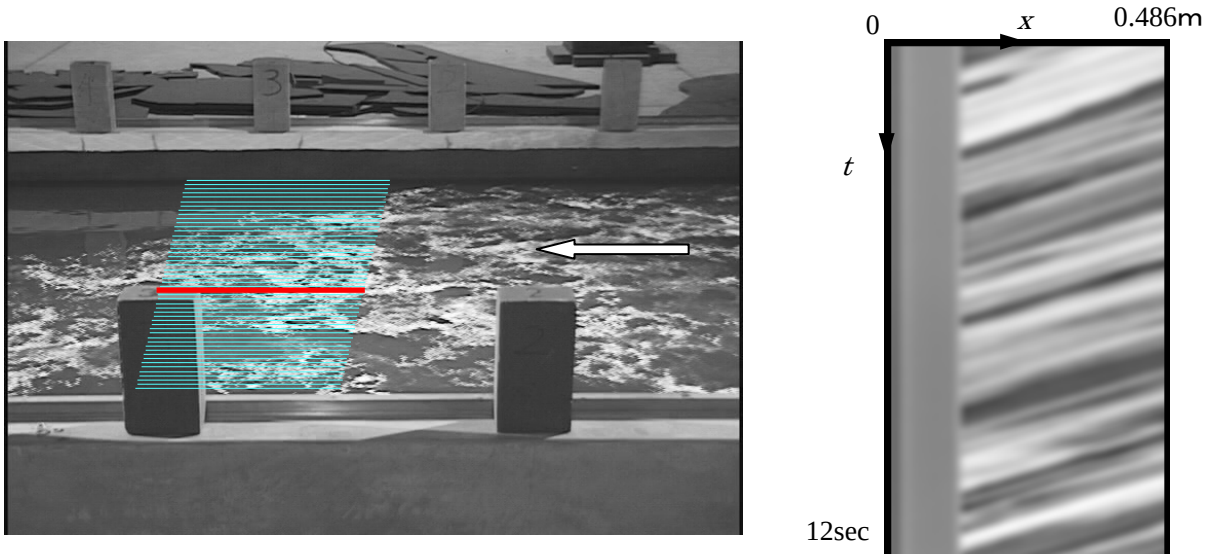

(a) (b)

Figure 2 Laboratory flume flow visualized by tracer; (a) oblique-angled image and the location of searching line (b) an example of STI for a thick searching line indicated in (a).

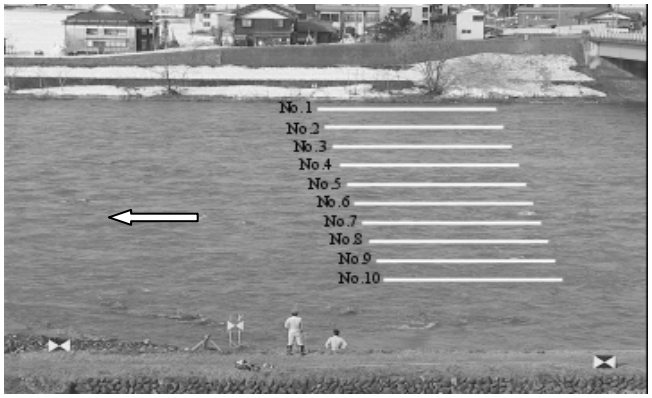

Figure 3 Surface flow image of flood flow of the Uono River and searching lines; the river surface width is about 100m.

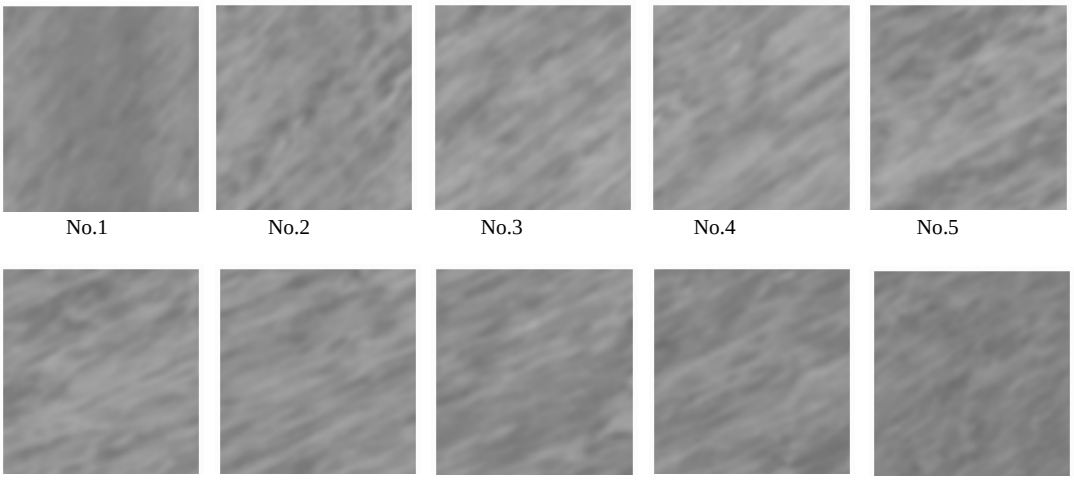

Figure 4 STIs for the searching lines indicated in figure 3; horizontal length is 200 pixels and vertical length corresponds to 6.7seconds.

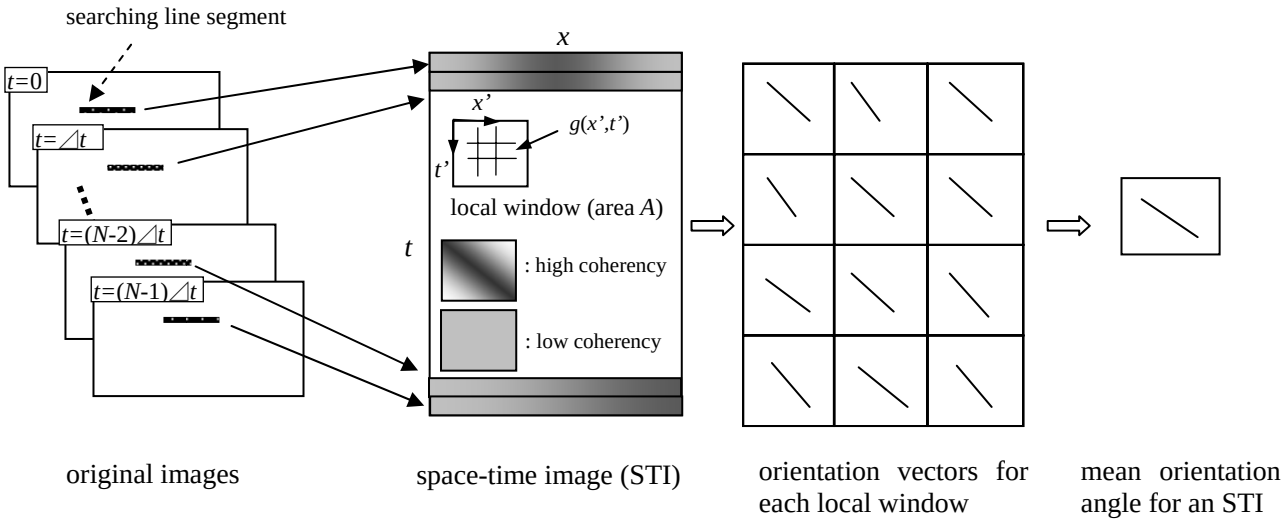

Figure 5 Outline of STV procedure.

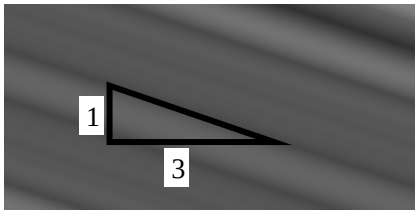

(a) Case V

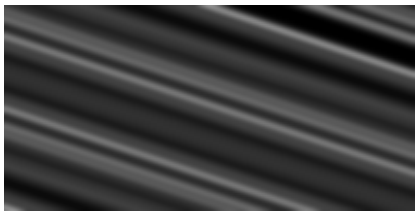

(b) Case C

Figure 6　Synthetic STI (tan ϕ = 3, 100 by 50 pixels).

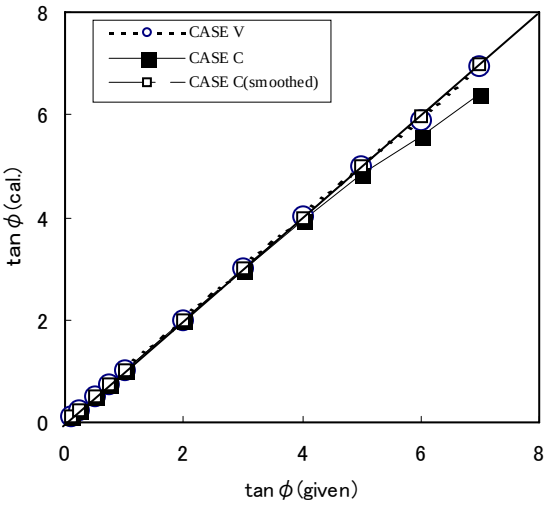

Figure 7　Comparison of calculated results.

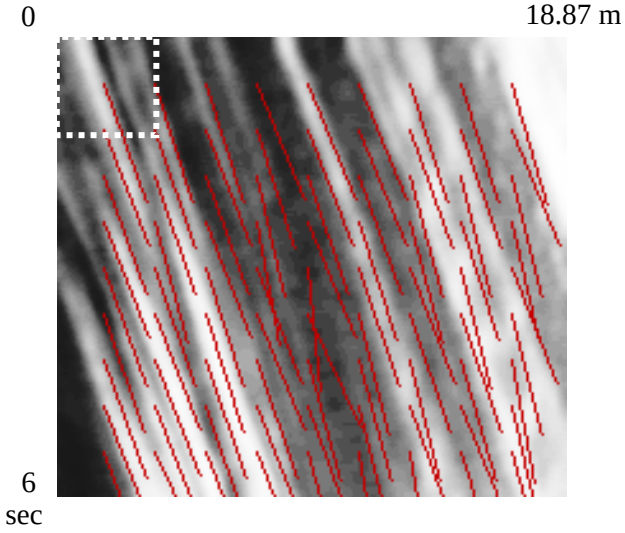

Figure 8 Orientation vectors obtained by STIV; the image is enhanced for clarity.

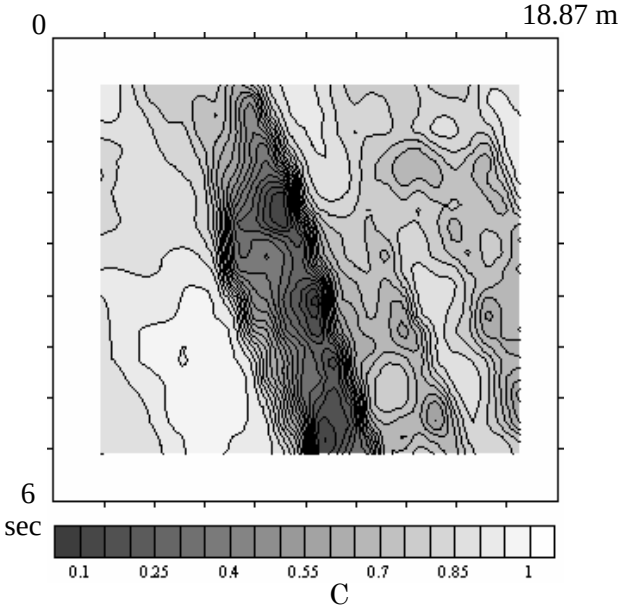

Figure 9 Distribution of coherency.

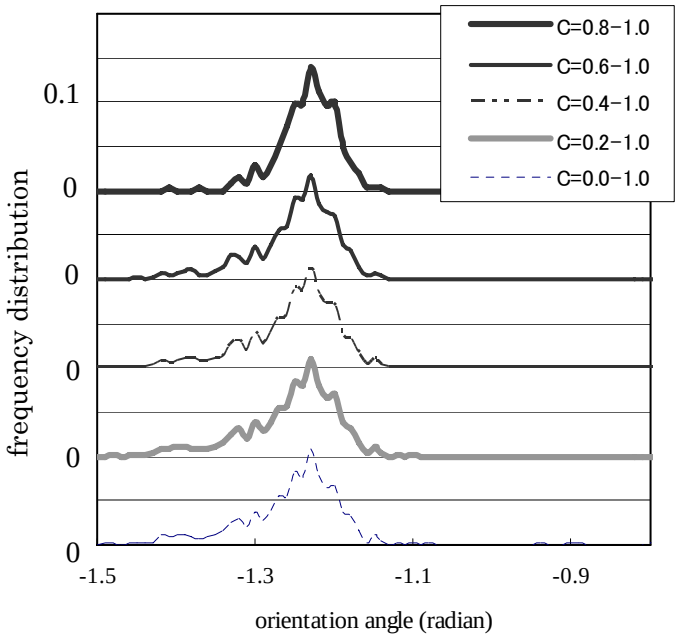

Figure 10 Frequency distribution of orientation angle for various coherency ranges.

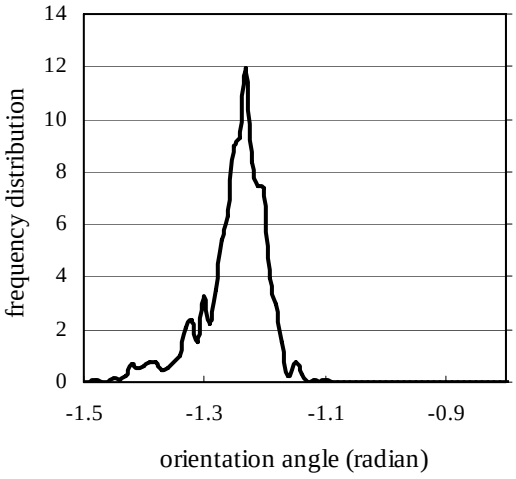

Figure 11 Frequency distribution of orientation angle after adding respective distribution.

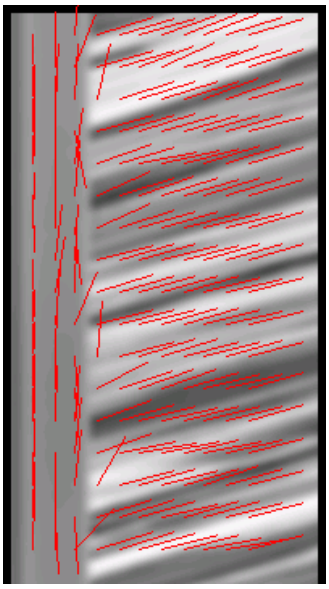

Figure 12 Distribution of orientation angles for STI affected by object.

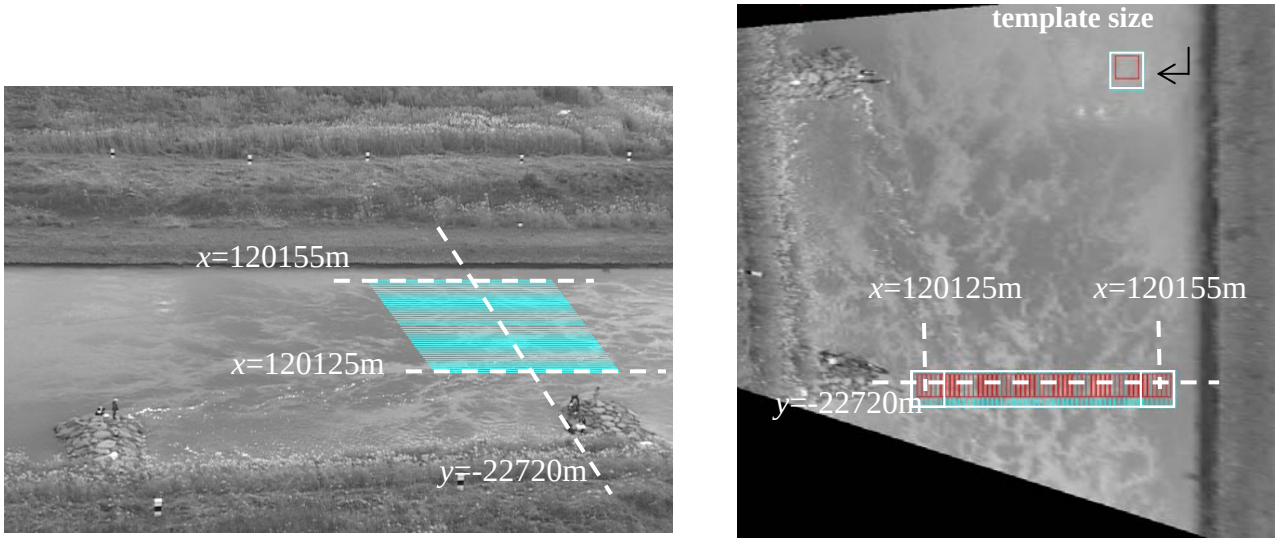

(a) original image; line segments are shown

(b) transformed image; image size is 700 x 700 pixels with pixel size of 0.1m

Figure 13 The original image used for STIV and the transformed image used for LSPIV.

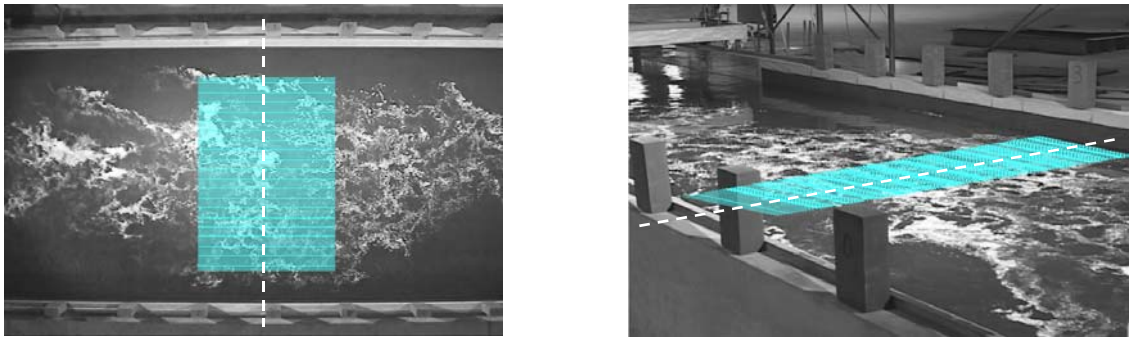

(a) angle A　　(b) angle C

Figure 14 Videotaped angles for flume experiments.

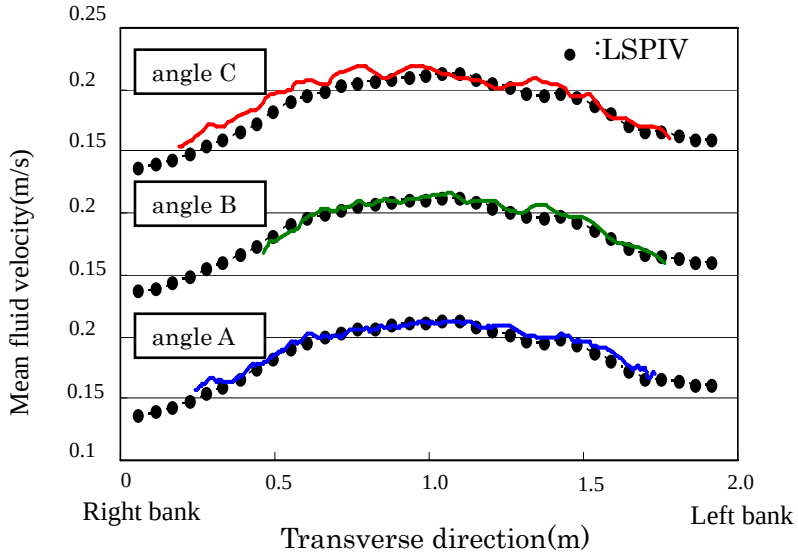

Figure 15 Surface velocity distributions measured by STIV and PIV for the flume experiment.

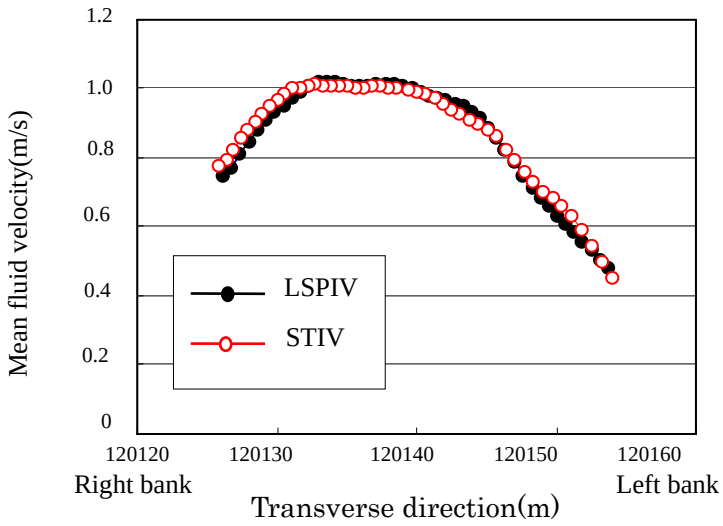

Figure 16 Comparison of cross-sectional distributions of streamwise velocity component measured by STIV and PIV for the Uji River.

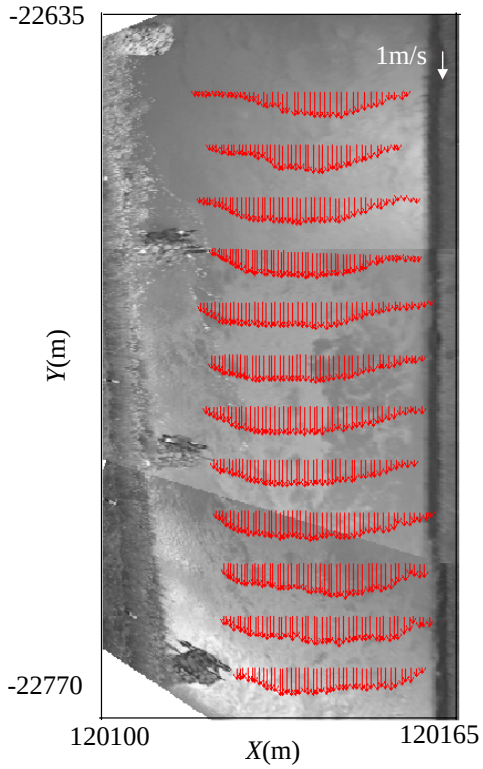

Figure 17 Streamwise velocity distribution of the Uji River measured by STIV.

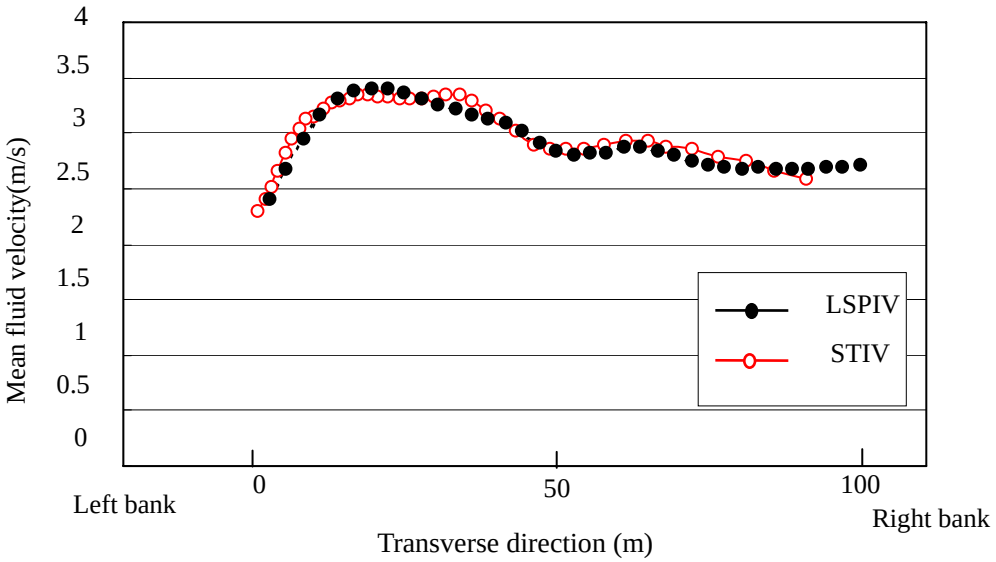

Figure 18 Streamwise velocity distribution measured by STIV for the Uono River flood flow.

Table 1 General feature of STIV and LSPIV.

	STIV	LSPIV
principle	gradient measurement	pattern matching
velocity comp.	1-D (flow direction)	2-D (free surface)
image plane	2-D (X-T plane)	2-D (X-Y plane)
spatial resolution	high in transverse	less than STIV
CPU load	small	large
camera setting	arbitrary	arbitrary
to noisy image	robust	less than STIV
viewing angle	allow small angle	require larger angle
system construction	easy to be automated	can be automated
low flow measurement	possible (use tracer)	possible (use tracer)